This is the peer reviewed version of the following article:

1 <div align="right">**Scientific paper**</div>

2

3 **Valorization of walnut shell ash as a catalyst for biodiesel production**

4

5 Marija R. Miladinović[1], Miodrag V. Zdujić[2], Djordje N. Veljović[3], Jugoslav B. Krstić[4], Ivana B.

6 Banković-Ilić[1], Vlada B. Veljković[1,5*], Olivera S. Stamenković[1]

7

8 [1] Faculty of Technology, University of Niš, Bulevar oslobođenja 124, 16000 Niš, Serbia

9 [2] Institute of Technical Sciences of the Serbian Academy of Sciences and Arts, Knez Mihailova

10 35, 11000 Belgrade, Serbia

11 [3] Faculty of Technology and Metallurgy, University of Belgrade, Karnegijeva 4, 11000 Belgrade,

12 Serbia

13 [4] Institute of Chemistry, Technology and Metallurgy, Center for Catalysis and Chemical

14 Engineering, University of Belgrade, Njegoševa 12, 11000 Belgrade, Serbia

15 [5] The Serbian Academy of Sciences and Arts, Knez Mihailova 35, 11000 Belgrade, Serbia

16

[*] Corresponding author: Vlada B. Veljković, Faculty of Technology, University of Niš, 16000 Leskovac, Bulevar oslobodjenja 124, Serbia; phone: +381 16 247203; fax: +381 16 242859; e-mail: veljkovicvb@yahoo.com

17   **Abstract**

18   The catalytic activity of the walnut shell ash was investigated in the biodiesel production by the

19   sunflower oil methanolysis. The catalyst was characterized by the TG-DTA, XRD, Hg

20   porosimetry, N_2 physisorption, SEM, and Hammett method. In addition, the effects of the

21   catalyst loading and the methanol-to-oil molar ratio on the methyl esters synthesis were tested at

22   the reaction temperature of 60°C. The walnut shell ash provided a very fast reaction and a high

23   FAME content (over 98%). As the reaction occurred in the absence of TAG mass transfer

24   limitation, the pseudo-first-order model was employed for describing the kinetics of the reaction.

25   The catalyst was successfully reused four times after the regeneration of the catalytic activity by

26   recalcination at 800 °C.

27   Keywords: ash; biodiesel; kinetics; methanolysis; sunflower oil; walnut shell.

28

1. Introduction

Biodiesel, a mixture of fatty acid alkyl esters, is obtained by the chemical reaction of oily raw materials (edible, non-edible, or waste vegetable oils, animal fats, or micro-algal lipids) with appropriate alcohol (usually methanol or ethanol). This reaction, named transesterification or alcoholysis, is usually realized in the presence of a suitable catalyst. The most commonly used catalysts are potassium and sodium hydroxide despite several problems associated with them. For instance, they cannot be recovered and reused after the reaction, must be neutralized at the end of the reaction by water washing, which generates a large amount of wastewater, and demand precautions for safe handling during operation and storage. A solution for these problems has been found in the application of heterogeneous catalysts such as alkali metal oxides as neat or loaded on the support. Their advantages over homogeneous catalysts refer to easy separation from the reaction mixture and the possibility to be reused. Moreover, since recently, the heterogeneous catalysts have been improved by loading the metals onto the catalyst surface to increase its hydrophobicity, which prevents the adsorption of water generated during the reaction and contributes to the catalyst stability [1,2]. On the other hand, the heterogeneously catalyzed reactions have a longer reaction time than homogenously catalyzed reactions. Besides that, some catalysts require a complex synthesis.

Since recently, to reduce the overall biodiesel production cost, appropriate solid catalysts have been prepared from waste materials such as agricultural wastes, sea materials and biodegradable parts of industrial and municipal wastes. A special attention has been paid to biomass-derived solid catalysts, such as ashes obtained from coconut husk [3], empty fruit bunch [4], *Lemna perpusilla Torrey* [5], rice husk [6-8], tucumã peel [9] and "red" banana peduncle [10]. Generally, the preparation of these catalysts involves drying and combustion (in the range 350–

52 900 °C) of biomass. In order to get more suitable catalysts, some ashes are used as a support for

53 active components like the bamboo leaf and coal fly ashes for ZrO_2 [11] and calcined animal

54 bone powder [12], respectively. Their preparation includes milling, impregnation of active

55 components, drying and calcination. Although better stability of these catalysts is achieved by

56 impregnation of the active component on the ash, the preparation method is more complex and

57 requires the use of solvents. Therefore, simple combustion was used in the present work to get

58 ash from waste walnuts shells, which may have practical applications.

59 The world productions of walnuts (in the shell) and walnut kernels are about 2,000.000 and

60 890.000 tons per year [13], respectively. Therefore, as a result of walnuts processing, a large

61 amount of waste walnut shells is generated, which can be a valuable source of energy. The

62 walnut shells (endocarp) contain lower contents of hygroscopic (cellulose and hemicellulose)

63 and higher contents of hydrophobic (lignin) components [14], which result in an "energy

64 content" comparable to that of coal [15] and more resistance to the moisture [16]. Besides energy

65 (heat/electricity), combustion of walnut shells generates ash as a solid waste that could find some

66 application as other ashes, for instance, as a catalyst, support for other catalytical species, or an

67 adsorbent.

68 So far, the walnut shell has been used for the preparation of activated carbon, which was

69 tested as an adsorbent for volatile organic compounds [17] and as a support for La and Ca

70 employed in biodiesel production [18]. However, the catalytic activity of walnut shell ash has not

71 been tested yet in transesterification reactions despite their chemical composition (with

72 dominated alkali and alkali earth elements) indicates the possibility of its utilization as a catalyst.

73 In addition, walnut shell ash has not been characterized completely as a solid catalyst.

4

74   This study deals with using ash, obtained by the air combustion of waste walnut shells, as a

75   catalyst in the methanolysis of sunflower oil, which has not been reported yet. The obtained ash

76   was characterized by the TG-DTA, XRD, Hg porosimetry, N_2 physisorption, SEM, and Hammett

77   method. In addition, the effects of the reaction conditions (the initial methanol-to-oil molar ratio

78   and catalyst loading) on methyl ester content were tested. Moreover, the kinetics of the

79   methanolysis reaction was analyzed. The catalyst reusability was also studied to estimate the

80   possibility of its commercial application. Therefore, the novelties of the present study are the

81   first use of the waste walnut shells ash as a catalyst for biodiesel production, the complete

82   characterization of the obtained ash including the evaluation of its reusability and the

83   development of a simple mathematical model describing the kinetics of the tested reaction.

84   **2. Materials and methods**

85   **2.1. Materials**

86   In experimental work, the refined sunflower seed oil (Dijamant, Zrenjanin, Serbia) and

87   methanol (purity of 99.5%; Zorka Pharma, Šabac, Serbia) were used. The oil consisted mainly of

88   palmitic (6.20%), stearic (3.09%), oleic (30.79%) and linoleic (58.89%) acid, making up about 99%

89   of the oil. The walnuts were obtained from a local market. Methanol, 2-propanol, and *n*-hexane,

90   HPLC purity, were from LGC Promochem (Wesel, Germany).

91   **2.2. Catalyst preparation**

92   The walnut shell fraction remaining after crushing the walnuts and removing the kernels was

93   combusted in the air, and the obtained biochar was cooled, ground, and calcined in a furnace at

94   800 °C in the air. The obtained walnut shell ash was used as the catalyst. The calcination

95 temperature was selected based on the TGA/DTA analysis. The spent catalyst was recalcined in

96 the same furnace at 800 °C for 2 h.

2.3. Catalyst characterization

98 The elemental analysis of walnut shell ash, spent and recalcined spent catalyst samples was

99 performed by an Oxford Inca 3.2 energy dispersive spectroscopy (EDS) coupled with a Jeol JSM

100 5800 scanning electron microscope (SEM) operated at 20 keV. Before the analysis, the powders

101 were affixed at the surface of graphite tape in the form of a thin layer. The thermal behavior was

102 determined by simultaneous TG/DTA measurement (Setsys, SETARAM Instrumentation,

103 Caluire, France) under a synthetic air flow in the temperature range from ambient temperature up

104 to 1200 ^{o}C at a heating rate of 20 ^{o}C min^{-1}, using an alumina pan. The X-ray powder diffraction

105 measurements were performed by a Philips PW 1050 X-ray powder diffractometer using Cu

106 K$\alpha_{1,2}$ (λ = 1.54178 Å) radiation in the 2θ range of 10–90°, step-length of 0.01° and the scan time

107 of 5 s. The morphology of the catalyst was observed by TESCAN MIRA 3 XMU field emission

108 scanning electron microscope (FE-SEM), operated at 20 keV. A thin gold layer was deposited on

109 the catalyst surface before analysis, in order to provide conductivity.

110 The textural properties of the walnut shell ash were determined by Hg intrusion porosimetry

111 and N$_2$ physisorption at 77 K. The bulk density was measured on a Macropore Unit 120 (Fisons

112 Instruments) using mercury as the displacing fluid. Prior to the analysis, the sample was dried in

113 an oven at 110 ^{o}C during 16 h and additionally evacuated in a sample holder at the analytical

114 position for 90 min. The Hg porosimetry measurement was performed on a high-pressure unit

115 PASCAL 440 (Thermo Fisher) within the pressure range 0.1−200 MPa. Two subsequent

116 intrusion–extrusion runs (Run1 and Run2) were conducted. An automatic data acquisition of

117 intrusion–extrusion Hg volume *versus* applied pressure values was obtained through an interface

118 SOL.I.D Software System collecting the data of the change in Hg volume with a resolution of

119 0.1 mm^3. Additionally, the SOLver Ver. 1.3.4 software was used for calculating the following

120 parameters: total intruded Hg volume, specific surface area, bulk density, apparent density, and

121 porosity.

122 Adsorption-desorption isotherm was obtained by N_2 adsorption at 77 K on a Sorptomatic

123 1990 Thermo Finnigan device. Prior to adsorption, the samples were outgassed for 2 h under

124 vacuum at room temperature and afterward at 300 ºC and the same residual pressure for 16 h.

125 The sample of the spent catalyst was pretreated to remove the reaction products from the catalyst

126 surface. The presence of the reaction products on the surface of the spent catalyst made the

127 measurement of the specific surface area by N_2 physisorption at 77 K unmanageable in respect of

128 accuracy of SSA determination and possible contamination of the instrument measuring line.

129 The sample of the spent catalyst was transferred into a cellular tumble and 44 extractions were

130 carried out in a Soxhlet apparatus using *n*-hexane. After extraction, the residual *n*-hexane was

131 removed by heating in an oven at 110 °C. Finally, the sample was transferred in a sample holder

132 and prepared for the N_2 measurement by the same procedure as the starting sample, i.e.

133 outgassed for 2 h under vacuum at room temperature and afterward at 300 ºC and the same

134 residual pressure for 16 h.

135 The specific surface area of the samples was calculated from the linear part of the adsorption

136 isotherm by applying the Brunauer-Emmett-Teller (BET) equation [19]. The micropore volume

137 was estimated by the Dubinin-Radushkevich method [20]. The mesopore volume and the

138 mesopore size distribution were estimated by the Barrett, Joyner, and Halenda (BJH) method

139 [21] from the desorption branch using the Lecloux standard isotherm [22].

140   The base strength of the catalyst was determined by the Hammett indicators method. The

141   following indicators were used: phenolphthalein (H_= 9.3), thymolphthalein (H_= 10.0), thymol

142   violet (H_= 11.0), and 2,4-dinitroaniline (H_= 15.0).

2.4. Transesterification

144   The transesterification was performed in a 250 mL three-necked glass round-bottomed flask,

145   equipped with a reflux condenser and a magnetic stirrer. The reaction flask was immersed in a

146   glass chamber filled with water circulating from a thermostated bath by means of a water pump

147   to maintain the temperature in the chamber constant at 60 ± 0.1 °C. The sunflower oil (20 g) was

148   transesterified with various amounts of methanol (corresponding to initial methanol-to-oil molar

149   ratio of 6:1, 12:1, or 18:1) over various amounts of walnut shell ash (catalyst amount of 0.5, 1,

150   2.5, or 5.0% of the oil weight) at the reaction temperature of 60 °C and the stirrer speed of 800

151   rpm for 2 h. During the reaction, the samples were periodically taken from the reaction mixture,

152   poured into plastic vials, which were immersed in the ice water and immediately centrifuged

153   (Sigma Laborcentrifugen 2-6E, Germany, 3500 rpm) for 10 min to separate the solid catalyst

154   particles. The upper methyl ester layer was withdrawn and dissolved in a solution of 2-propanol

155   and *n*-hexane (5/4, v/v) in the ratio of 1:200 and filtered through a 0.45 μm Millipore filter. The

156   filtrate was used for the chemical composition analysis by HPLC method as described elsewhere

157   [23]. All experiments were performed in duplicate.

2.5. Crude biodiesel purification

159   The final reaction mixture was centrifuged at 3500 rpm for 10 min to separate the methyl

160   ester phase from the alcoholic phase and the solid catalyst. The upper methyl ester phase was

161   decanted and subjected to purification. For this purpose, the three different methods were

162   employed: (a) washing with distilled water, (b) Alba Rubio and coworkers' method [24] and (c)

163   extraction with deep eutectic solvents (DES) choline chloride:glycerol:ethylene glycol (1:2:1), as

164   suggested by Hui Min et al. [25], and choline chloride:glycerol (1:2).

165   (a) The upper methyl ester phase was mixed with the distilled water at a volume ratio of 4:1

166   mL/mL for 30 min at 500 rpm and room temperature, followed by centrifugation to separate

167   the washed methyl esters, which was then dried in an oven at 105 °C to a constant weight.

168   (b) The upper methyl ester phase was washed with methanol (50% based on the crude methyl

169   esters mass) containing anhydrous sodium carbonate (5% based on the crude methyl esters

170   mass) at 65°C for 4 h under agitation by a magnetic stirrer (1000 rpm). After the gravitational

171   separation and filtration, the methyl ester phase rinsed with distilled water (10% of methyl

172   esters mass, 25 °C) under agitation (500 rpm) for 1 h. The aqueous phase was decanted after

173   gravitational separation from the methyl ester phase, which was then dried by adding

174   anhydrous sodium sulfate. The final mixture was filtered to separate the purified methyl

175   esters.

176   (c) The upper methyl ester phase was mixed (200 rpm) with the choline

177   chloride:glycerol:ethylene glycol (1:2:1) DES at molar ratio 1:0.5 for 1 h at 25 °C. The

178   methyl ester phase was gravitationally separated from DES [25]. The same procedure was

179   repeated when the choline chloride:glycerol was used.

180   **2.6. Theoretical part**

181   Although the transesterification of sunflower oil (i.e. mainly a mixture of triacylglycerols,

182   TAGs) with methanol occurs *via* three consecutive reversible reactions forming diacylglycerols

183   (DAGs), monoacylglycerols (MAGs), fatty acid methyl esters (FAMEs), and glycerol, the

184   following overall reaction has frequently used for the purpose of the kinetic modeling:

185 $A + 3B \rightleftharpoons 3R + S$ (1)

186 where **A** is TAGs, **B** is methanol, **R** is FAMEs, and **S** is glycerol.

187 For the purpose of kinetic modeling the following assumptions were adopted:

188 a) The disappearance rate of DAGs and MAGs was higher than the disappearance rate of

189 TAGs, which was proved by their low concentrations in the reaction mixture. The

190 concentration of DAGs and MAGs were almost constant as the reaction progressed.

191 b) The reaction occurred in the absence of the TAG mass transfer limitation, i.e. in a pseudo-

192 homogeneous regime, allowing the use of the following kinetic pseudo-first-order model:

193 $(-r_A) = -\dfrac{dc_A}{dt} = k_{app} \cdot c_A$ (2)

194 where c_A is the TAG concentration, k_{app} is the apparent rate reaction constant, and t is the

195 reaction time. Further, if the TAG concentration is expressed through TAG conversion

196 degree x_A, i.e. $c_A = c_{A0} \cdot (1 - x_A)$, then after integration with the initial condition: $t = 0$ and x_A

197 = 0, the following equation is obtained:

198 $-\ln(1 - x_A) = k_{app} \cdot t$ (3)

199 c) The reaction mixture was perfectly mixed by vigorous agitation.

200 d) The neutralization reaction was ignored due to a negligible free fatty acid content in the oil.

201 **3. Results and discussion**

202 **3.1. Catalysts characterization**

203 The TG and DTA curves of walnut biochar are presented in Fig. 1. In the range from the

204 ambient temperature to 330 °C, a slight weight loss of only 4% was observed, which was

205 attributed to the removal of moisture and light molecular weight compounds [26]. The main

206 decomposition occurred in the range 330–850 °C where the weight loss was 93.6%, which was

207 attributed to the decomposition of hemicelluloses, celluloses, and lignin at 220–315 °C, 315–400

208 °C, and 160–900 °C, respectively [27]. Luque et al. [28] reported that most of the carbon species

209 were decomposed in the range 400–800 °C in the air. The temperature of 800 °C was high

210 enough to enable the transition from a carbonaceous material to the material composed mostly of

211 metal oxides.

212 <div align="center">Fig. 1.</div>

213 The XRD patterns of the walnut shell biochar and ash are shown in Fig. 2a and b. A

214 characteristic wide peak (hump) in the $10–37^o$ 2θ range indicated a dominantly amorphous

215 structure of the biochar (Fig. 2a). In addition, the peak at 29.7^o suggested the presence of some

216 crystalline phase embedded in the amorphous matrix. After calcination at 800 ^{o}C, the XRD

217 revealed a crystalline material, resulting from the thermal decomposition (Fig. 2b). The peaks at

218 32.58, 37.62, 54.17, 64.69, 67.88, 79.08, and 88.63^o corresponded to the CaO phase (PDF#82-

219 1690), the peaks at 43.15 and 82.69^o might be assigned to the MgO (periclase) phase (PDF#78-

220 0430),while the peaks at 22.50, 30.68, 43.17, and 67.88^o could be tentatively assigned to the

221 SiO_2 (β-cristobalite) (PDF#89-3607) and the peaks at 25.52, 30.67 and 51.23^o as a result of solid-

222 state reaction at 800 ^{o}C to the K_2O (PDF#77-2176). Besides, as a result of solid-state reaction at

223 800 ^{o}C, the calcined walnut ash plausibly contained dicalcium silicate, Ca_2SiO_4 (PDF#52-0809),

224 indicated by the peaks at 90.80, 41.79, and 60.47^o, and $KAlO_2$ (PDF# 53-0809), indicated by the

225 peaks at 32.57 and 58.21^o, respectively. The peaks at about 18.25 and 34.32^o were assigned to

226 $Ca(OH)_2$ (portlandite, PDF#44-1481), which was formed by a reaction of CaO with water from

227 the air. However, some other phases, such as Na_2O, or, for example, $K_4H_2(CO_3)_3 \cdot 1\frac{1}{2} H_2O$ and

228 $KHSi_2O_5$ as found in miscanthus ash [29] could not be excluded.

229   Generally, the detected crystalline phases were also found in the other types of biomass

230 residue after combustion/calcination. For instance, the crystalline CaO phase was present in the

231 materials obtained from biomass residues by gasification and calcination [28]. Also, when a

232 higher calcination temperature was applied, the content of K and Ca in the material was found to

233 be higher at the expense of carbon due to a greater mass loss attributed to the removal of

234 carbonaceous species and the decomposition of other recalcitrant species of material [28].

235   Fig. 2.

236   The elemental composition of walnut shell ash was determined by the EDX method. The

237 highest content of K (23.55 wt.%) and Ca (17.67 wt.%) was detected, indicating their major role

238 in the catalysis. The presence of other elements was insignificant. However, Vassilev et al. [30]

239 reported Ca, K, and Si as the most abundant elements in another walnut shell ash. This indicates

240 that the elemental composition of walnut shell ashes can vary with the geographical region and

241 cultivation conditions.

242   The textural parameters of walnut shell ash, obtained by the Hg porosimetry and N_2

243 physisorption measurements, are given in Table 2. In addition, the total intruded volume of Hg

244 for the two consecutive runs (Run1 and Run2) and the corresponding pore distribution is shown

245 in Fig. 3. The most obvious difference between the two runs was the significant reduction of the

246 total volume in the Run2, which was only about 40% of the total value obtained in the Run1.

247 Also, the maximum of the pore size distribution (PSD) curve shifted to the smaller values (from

248 5.6 μm for the Run1 to 1.2 μm for the Run2). For the powder materials, during the first Hg

249 intrusion cycle, the mercury filled up both the interparticle (voids) and intraparticle spaces, while

250 in the second cycle of the measurement, Hg could occupy only the space of the accessible pores

251 (intraparticle space) [31]. Therefore, the obtained difference in the total intruded Hg volume, for

252 the two consecutive measurements, indicated a significant interparticle space present in the

253 material, which increased the total porosity of the analyzed sample. Since the porosity

254 represented the ratio of the total intruded Hg volume and the bulk volume of the material (per

255 gram of material), it became clear why the porosity for the second measurement was reduced

256 from 26.9% (Run1) to a relatively low value of 11.8% (Run2). Although the accessible volume

257 for the Run2, in the overall range of the diameters (13 μm to 7.5 nm) is not large (65 mm^3/g), the

258 results clearly showed that there was a real network of micron, submicron and nanometer pores

259 in the examined walnut shell ash calcined at 800 ^{o}C. This pore system derived from a system of

260 stable agglomerates of micron and submicron dimensions, which can be recognized on the SEM

261 micrographs recorded at 10,000 magnification (Fig. 4a). The higher magnification of 50,000

262 (Fig. 4b) revealed even smaller, tightly packed needle-like structures, which were formed during

263 the thermal treatment at 800 ° C. The existence of voids in these structures is clearly visible.

264 Despite the differences in the intruded Hg volume and the position of the maximum on the

265 distribution curve for the first and second cycle measurement in the macropore region (pore

266 diameter >50nm), the shape of the intrusion curves and the total volume of the intruded Hg in the

267 mesoporous region were almost the same for both measurements. Both distribution curves have

268 several maximums in the region of 7.5–20 nm. Although their positions do not necessarily

269 correspond to the real values of the pore diameter in the tested material (due to the small

270 measured volume changes), their presence is clear evidence of the mesopores existence in the

271 analyzed ash sample, at least to some extent. Also, the ascending trend of the Hg intrusion curve,

13

272 for the smallest measured diameters indicates a possible presence of pores less than 7.5 nm in

273 diameter.

274   Fig. 3. and Fig. 4.

275   The walnut shell ash was additionally characterized by the physisorption of N_2 at 77 K. The

276 results of this characterization are given in Table 1 while the adsorption-desorption isotherm is

277 displayed in Fig. 5. The shape of the isotherm with a plateau indication on the desorption branch

278 at the relative pressure of ≈ 0.9 and the presence of a hysteresis loop, despite the small values of

279 the specific surface (S_{BET} = 8.8 m^2/g), confirmed the presence of the mesopores in the test

280 sample. The low values of the specific surface area could be expected due to the particle

281 agglomeration during the high-temperature treatment. During this process, the decomposition of

282 the carbonaceous material occurred and its transition to the crystalline phase of metal oxides led

283 to the formation of particle agglomerates at high temperature.

284   Table 1., Fig. 5.

285   The insert in Fig. 5 shows the content of the pores in the mesoporous region and their

286 distribution calculated by the BJH method. The presence of mesopores smaller than 7.5 nm is

287 clearly visible. On the other hand, the content of the micropore, calculated according to the

288 Dubinin-Radushkevich method, is negligible, so this type of porosity does not have any

289 significant impact on the overall textural characteristics of the analyzed ash. Finally, from the

290 data of the N_2 physisorption measurements, it was possible to extract only the pore volume

291 fraction which was inaccessible to the Hg porosimetry measurement (pore diameter < 7.5 nm);

292 this overall volume was 10 mm^3/g. Adding this value to the pores volume obtained from the Run

293 2 by the Hg porosimetry, the determined total pore volume of the walnut shell ash was found to

294   be 0.075 mm^3/g. The corresponding total porosity, which originated exclusively from the whole

295   pores system and not from interparticle voids, was 13.6%.

296   Based on the Hammett indicator tests, the basic strength of walnut shell ash was in the range

297    $11 < H\_ < 15$. The total basicity was 0.352 mmol g^{-1}. Chen et al. [7] were reported higher total

298   basicity and base strength of a rice husk ash calcined at a higher temperature.

3.2. Sunflower oil methanolysis tests

300   Fig. 6 illustrates the variation of the FAME content in the ester-oil phase during the sunflower

301   oil methanolysis over walnut shell ash as a catalyst. TAGs were transformed very quickly (in the

302   first 10 min) into FAMEs, indicating the absence of the TAG mass transfer limitation. Such

303   behavior could probably be attributed to the nature of the solid catalyst. The MAG and DAG

304   contents were low and almost constant during the reaction, confirming the assumption (a).

305   Therefore, the influence of catalyst loading on the FAME synthesis was investigated first.

306   The influence of the catalyst loading (0.5, 1.0, 2.5, and 5.0% of the oil weight) on FAME

307   content was investigated at the initial methanol-to-oil molar ratio of 12:1 and the reaction

308   temperature of 60 °C under the atmospheric pressure. As can be seen in Fig. 6a, the FAME

309   content over 95% was reached for 2 h at the lowest catalyst loading (0.5% of the oil weight). The

310   further increase of the catalyst loading increased the reaction rate and reduced the reaction time

311   needed to reach the maximum FAME content (98%). This was attributed to the pseudo-

312   homogeneous nature of walnut shell ash. A higher catalyst loading provided a higher

313   concentration of catalytic species (Ca^{2+} and K$^+$) in the reaction mixture and higher dispersion of

314   active basic sites on the catalyst surface, thus accelerating the reaction. The similar nature of

315   empty fruit bunch ash was observed by Boey et al. [4] in the palm olein transesterification. In

316 addition, the increase of the catalyst concentration over 3% reduced FAME content, which was

317 ascribed to the mass transfer problems [4]. At the loading of 3%, the calcined wood ash [32] and

318 the calcined date seeds [33] provided the highest ester conversion of 97.7% and yield 96.1%,

319 respectively. Using a lower loading (1%) of the catalyst prepared from rice husk and Li_2CO_3 in

320 the molar ratio of 1:4 by grinding and calcining at 800 °C, Dai et al. [34] achieved a high

321 biodiesel conversion degree (98.8%) at a higher reaction temperature (65 °C) for a longer

322 reaction time (3 h). According to statistical evaluation, the concentration of calcined "red"

323 banana peduncle used as a catalyst was the most influential parameter among of the reaction

324 conditions [10].

325 The sunflower oil methanolysis reaction catalyzed by walnut shell ash was completed within

326 10 min when the catalyst loading was higher than 1%. Therefore, the influence of methanol-to-

327 oil molar ratio on FAME synthesis was investigated at a catalyst loading of 1% (Fig. 6b). With

328 the methanol-to-oil molar ratio of 6:1, the FAME content of 97.87% was achieved within 40

329 min. The increase of the methanol-to-oil molar ratio to 12:1 increased the rate of the FAME

330 synthesis and the reaction completed within 30 min, providing the 96.5% FAME content. The

331 reaction time to reach the FAME content over 90% at a higher methanol-to-oil molar ratio (18:1)

332 was only 10 min. Similarly, Vadery et al. [3] reported that the FAME content increased with

333 increasing the methanol-to-oil molar ratio, reaching above 95% at the methanol-to-oil molar ratio

334 of 12:1. The oily feedstock conversion increased with increasing the methanol-to-oil molar ratio

335 in the transesterification of palm olein catalyzed by boiler ash [4]. The highest conversion of

336 palm olein was obtained at the methanol-to-oil molar ratio of 15:1 while a further increase did

337 not affect the conversion. Mendonça et. al. [9] was also found the optimal methanol-to-oil molar

338 ratio of 15:1. On the other hand, when the waste materials such as palm mill fly ash [35] and rice

339 husk ash [7] were used as supports for CaO, the positive effect of increasing the methanol-to-oil

340 molar ratio on FAME yield and TAG conversion was observed up to 12:1 and 9:1, respectively.

341 The increase of the methanol-to-oil molar ratio above these values reduced the FAME yield and

342 TAG conversion.

343 Fig. 6.

344 **3.3. Kinetic analysis and simulation of sunflower oil methanolysis**

345 The sunflower oil methanolysis catalyzed by walnut shell ash occurred in the pseudo-

346 homogeneous regime where the chemical reaction determined the overall reaction rate. The

347 apparent reaction rate constant (k_{app}) was calculated from the slope of the linear dependence of

348 $-\ln(1-x_A)$ versus reaction time (Table 2). Since the R^2 values for the obtained linear dependences

349 were high (0.96-0.99), the pseudo-first-order model was proved and used to describe the kinetics

350 of the sunflower oil methanolysis reaction over walnut shell ash showing the low (<10%) mean

351 relative percent deviation (MRPD).

352 Table 2.

353 The effect of methanol-to-oil molar ratio on the FAME synthesis was not investigated for

354 catalyst loading over 1% since the reaction was completed within 10 min. Therefore, only the

355 effect of catalyst loading on the apparent reaction rate constant was considered. It was observed

356 that the apparent reaction rate constant increased proportionally with the increase of the catalyst

357 loading, i.e.

358 $k_{app} = k \cdot c_{cat}$ (4)

359 where c_{cat} is the catalyst concentration and k is the reaction rate constant, which was determined

360 to be 0.526 L/(mol·min) ($R^2 = 0.96$).

361   The predicted TAG conversion degree was calculated using the developed pseudo-first order

362 kinetic model. The following equations were applied for the pseudo-homogeneous regime:

363   $x_A = 1 - \exp\left(-k_{app} \cdot t\right)$.   (5)

364 A very good agreement between the predicted and experimental values of TAG conversion

365 degree can be observed in Fig.7; it was also confirmed by a low MRPD of ±6.2% (based on 64

366 data).

367   Fig. 7.

368 **3.4. Comparison of catalytic activity of walnut shell ash and conventional catalysts**

369   The catalytic activity of walnut shell ash in the sunflower oil methanolysis reaction was

370 compared with that of the conventional catalysts, such as sodium and potassium hydroxide. As

371 can be seen in Fig. 8, the reaction over walnut shell ash was initially slightly slower than the

372 reactions catalyzed by alkali hydroxides (up to 5 min). However, the maximum TAG conversion

373 was reached within 10 min of the walnut shell ash-catalyzed reaction. These results showed that

374 walnut shell ash could be successfully used as a substitute for the conventional catalysts (sodium

375 and potassium hydroxide) in the oil methanolysis.

376   Fig. 8.

3.5. Catalyst reusability

Catalyst reusability was tested at the initial methanol-to-oil molar ratio of 12:1 and the catalyst loading of 5%. The catalyst loading of 5% was used to provide enough amount of the spent catalyst for subsequent reactions as a part of the spent catalyst was lost during its separation after each reaction. After the methanolysis was completed, the solid catalyst was separated from the reaction mixture by filtration and reused without any treatment. The results showed that FAME content drastically decreased, reaching only 5% and 33.4% within 10 min and 30 min, respectively (Fig. 9). In order to explain the drop of the catalytic activity, the catalyst was separated from the reaction mixture again and reused after calcination at 800 °C for 2 h. It was found that catalyst regained its catalytic activity by recalcination (Fig. 9). XRD patterns of the spent and recalcined spent catalyst are presented in Fig. 2c and d. The significant structural changes of the catalyst during the methanolysis reaction can be seen. Diffraction lines at 13.3, 20.6, 26.7 28.0, 34.0, 40.5 and 41.8 may be assigned to potassium calcium carbonate (fairchildite), $K_2Ca(CO_3)_2$ (PDF#83-1921), as a dominant phase (Fig. 2c) while the other phases such as $KAlO_2$, MgO, $Ca_{0.5}Mg_{0.5}O_3$ (dolomite) and CaO (lime) are present in significantly smaller amounts. Therefore, these structural changes may be one of the reasons for catalyst deactivation. Upon recalcination of the spent catalyst, the phase composition resembles the starting (as-prepared) walnut shell ash (see Fig. 2d). At high temperatures, potassium calcium carbonate (fairchildite) decomposed, individualizing both carbonates that further decomposed into their oxides and CO_2 [36], restoring the catalytic activity. The SEM micrographs of the spent catalyst (Figs 4c and d) show the disappearance of the observed needle-like structures that could be ascribed to the change of chemical nature of the dominant phase. As it can be observed in Fig 4e and f, during recalcination of the spent catalyst (800 °C for 2 h), the carbonates were

400 transformed into metal oxides as a dominant phase and the needle-like structures appeared again.

401 Although the catalytic activity was regained, the specific surface area decreased significantly

402 after recalcination compared to the spent and fresh catalysts (Table 1), The recalcination may

403 cause the collapse in the pore structure, decreasing the specific surface area and pore volume [4].

404 However, Boey et al. [4] confirmed that the specific surface area and porosity did not have a

405 significant effect on FAME content.

406 <div align="center">Fig. 9.</div>

407 The reusability test was also performed with the catalyst calcined after separation from each

408 of consecutive four batches to determine how many times the catalytic activity could be regained

409 by calcination. The results showed that FAME content decreased in the first 10 minutes of the

410 reaction during each batch, but the reaction was completed in 30 min in all batches (Fig. 10).

411 This can be explained by leaching the catalytic active species during the first and the second

412 reaction. The decrease of potassium content in the spent and recalcined spent catalyst samples

413 was confirmed by EDX analysis (Fig. 11). The high content of potassium was also detected in

414 the crude ester phase, which probably originated from the catalyst leaching (see section 3.6). On

415 the other hand, the calcium content was the highest in the recalcined spent catalyst. Further

416 investigation is needed to explain the observed increase of the calcium content after recalcination

417 of the spent catalyst. Table 3 compares the reusability of different ashes, obtained by combusting

418 waste plant materials, as a catalyst in biodiesel production. Generally, these ashes can be reused

419 up to five times probably due to different contents of the constitutional elements.

420 <div align="center">Fig. 10, Fig. 11, Table 3.</div>

3.6. Biodiesel characteristics

It was found that the content of calcium and magnesium in the crude ester phase was above the standard limit (11.1 ppm) but the higher content of potassium (2566 ppm) was detected, requiring a further purification of the ester phase. As can be seen in Table 4, the best results for the content of both calcium/magnesium and potassium/sodium were achieved by the washing of the ester phase with distilled water in volume ratio 4:1 mL/mL. The method of Alba Rubio and coworkers reduces the content of calcium/magnesium below 5 ppm but the potassium/sodium content still was very high and above the allowed limit.

Table 4.

The extraction method with DES was also unsuccessful for potassium removing from the crude methyl esters. It was found that both choline chloride:glycerol:ethylene glycol (1:2:1) and choline chloride:glycerol at methyl esters:DES molar ratio 1:0.5 did not have any effect on the potassium removal from the ester phase obtained by sunflower oil methanolysis. This disagreed with the findings of Hui Min et al. [15], who reported that the choline chloride:glycerol:ethylene glycol (1:2:1) was the most efficient among the employed DES in the potassium removal efficiency from the palm oil-based biodiesel at the biodiesel:DES molar ratio of 1:0.5. This showed that the employed biodiesel:DES molar ratio was probably not adequate and should be optimized in order to reduce the potassium content. In addition, the content of calcium/magnesium, although reduced with both DESs, was still above the standard limit.

Then, the purified ester phase was characterized according to the specific requirements of the biodiesel quality standard EN 14214 (Table 5). The obtained values of tested properties were within the standard EN 14214.

443   Table 5.

444   Conclusion

445   A catalyst in the ash form efficient for the sunflower oil methanolysis was prepared by

446   calcination (at 800 °C) of the walnut shell biochar remained after the conventional combustion.

447   The catalyst consists of the metal oxide (mainly CaO and K_2O), implying its base nature. The

448   increase of catalyst loading and methanol-to-oil molar ratio increased the reaction rate and

449   reduced the reaction time needed to reach the highest FAME content. The reaction catalyzed by

450   the highest catalyst loading (5%) at the methanol-to-oil molar ratio of 12:1 and the temperature

451   of 60 °C provided the FAME content above 98% within 10 min. This indicated the walnut shell

452   ash can successfully substitute sodium and potassium hydroxide as a catalyst. The kinetics of the

453   walnut shell ash-catalyzed methanolysis was described by the model of pseudo-first order

454   reaction. The catalyst activity declines after reuse without reactivation, but it was successfully

455   regained by recalcination at 800 °C for 2 h.

456   As an energy-intensive process, the calcination at 800 ^oC might be an obstacle for using

457   walnut shell ash as a catalyst. The proposed process of catalyst preparation from waste walnut

458   shells involves their air combustion that generates heat/electricity and may partly compensate for

459   the calcination cost. Also, the costs of disposal of walnut shell ash are avoided, thus further

460   compensating for the calcination cost. This waste can be considered no- or low-cost raw

461   material, depending on the transportation and handling costs. Compared to the traditional

462   homogeneous base catalysts (for instance, alkali hydroxides), the walnut shell ash-based catalyst

463   has all benefits of solid catalysts, such as easy separation from the reaction mixture, reusability

464   and lower amounts of wastewater, which positively affect the overall biodiesel production costs.

465   In comparison with many solid catalysts obtained by the complex synthesis, the preparation of

466 the walnut shell ash-based catalyst is much simpler. However, the definitive conclusion about the

467 best type among the above-mentioned catalyst can be given after a thorough techno-economic

468 analysis.

473

474 **Nomenclature**

475 c_A — Concentration of TAG, *mol/L*

476 c_{A0} — Initial concentration of TAG, *mol/L*

477 c_{cat} — Catalyst concentration, *mol/L*

478 k_{app} — Apparent reaction rate constant, *min^{-1}*

479 k — Reaction rate constant, L/(mol·min)

480 $(-r_A)$ — TAG reaction rate, *mol/(L·min)*

481 t — Reaction time, *min*

482 x_A — TAG conversion degree, 1

483

484   **Reference**

485   [1] Osman AI, Abu-Dahrieh JK, Rooney DW, Thompson J, Halawy SA, Mohamed MA, Surface

486   hydrophobicity and acidity effect on alumina catalyst in catalytic methanol dehydration

487   reaction, J Chem Technol Biotechnol 2017;92: 2952–2962. doi: 10.1002/jctb.5371.

488   [2] Osman AI, JK, Abdelkader A, Hassan NM, Laffir F, McLaren M, Rooney D. Silver-

489   Modified η‑Al2O3 Catalyst for DME Production. J Phys Chem C 2017; 121:25018-25032.

490   doi:10.1021/acs.jpcc.7b04697

491   [3] Vadery V, Narayanan BN, Ramakrishnan RM, Cherikkallinmel SK, Sugunan S, Narayanan

492   DP, Sasidharan S. Room temperature production of jatropha biodiesel over coconut husk ash.

493   Energy 2014;70:588-94. doi:10.1016/j.energy.2014.04.045.

494   [4] Boey PL, Ganesan S, Lim SX, Lim SL, Maniam GP, Khairuddean M. Utilization of BA

495   (boiler ash) as catalyst for transesterification of palm olein. Energy 2011;36:5791-6.

496   doi:10.1016/j.energy.2011.09.005.

497   [5] Chouhan APS, Sarma AK. Biodiesel production from *Jatropha curcas* L. oil using *Lemna*

498   *perpusilla* Torrey ash as heterogeneous catalyst. Biomass Bioenerg 2013;55:386–9.

499   doi:10.1016/j.biombioe.2013.02.009

500   [6] Chen KT, Wang JX, Dai YM, Wang PH, Liou CY, Nien CW, Wu JS, Chen CC. Rice husk

501   ash as a catalyst precursor for biodiesel production. J Taiwan Inst Chem Eng 2013;44:622–9.

502   doi:10.1016/j.jtice.2013.01.006.

503 [7] Chen GY, Shana R, Shi JF, Yan BB. Transesterification of palm oil to biodiesel using rice

504   husk ash-based catalysts. Fuel Process Technol 2015;133:8–13.

505   doi:10.1016/j.fuproc.2015.01.005.

506 [8] Roschat W, Siritanon T, Yoosuk B, Promarak V. Rice husk-derived sodium silicate as a

507   highly efficient and low-cost basic heterogeneous catalyst for biodiesel production. Energy

508   Convers Manag 2016;119:453–62. doi:10.1016/j.enconman.2016.04.071.

509 [9] Mendonça IM, Paes OARL, Maia PJS, Souza MP, Almeida RA, Silva CC, Duvoisin SJr, de

510   Freitas FA. New heterogeneous catalyst for biodiesel production from waste tucumã peels

511   (*Astrocaryum aculeatum* Meyer): Parameters optimization study. Renew Energ

512   2019;130:103-10. doi:10.1016/j.renene.2018.06.059.

513 [10] Balajii M, Niju S. A novel biobased heterogeneous catalyst derived from *Musa acuminate*

514   peduncle for biodiesel production‑Process optimization using central composite design.

515   Energy Convers Manag 2019;1:118‑131. doi: 10.1016/j.enconman.2019.03.085.

516 [11] Fatimah I, Rubiyanto D, Taushiyah A, Najah FB, Azmi U, Sim Y-L. Use of ZrO2 supported

517   on bamboo leaf ash as a heterogeneous catalyst in microwave-assisted biodiesel conversion.

518   Sustainable Chem Pharm 2019;12:100-129. doi: 10.1016/j.scp.2019.100129.

519 [12] Volli V, Purkait MK, Shu C-M. Preparation and characterization of animal bone powder

520   impregnated fly ash catalyst for transesterification. Sci Total Environ 2019;669:314–321.

521   doi:10.1016/j.scitotenv.2019.03.080.

522 [13] Herreros BF. XXXVII World Nut and Dried Fruit Congress, Sevilla, Spain, May 21-23,

523   2018.

524   [14] Vassilev SV, Baxter D, Andersen LK, Vassileva CG, Morgan TJ. An overview of the

525   organic and inorganic phase composition of biomass. Fuel 2012; 94:1–33.

526   doi:10.1016/j.fuel.2011.09.030.

527   [15] Mendu V, Harman-Ware AE, Crocker M, Jae J, Stork J, Morton III S, Andrew Placido A,

528   George Huber G, Seth DeBolt S. Identification and thermochemical analysis of high-lignin

529   feedstocks for biofuel and biochemical production. Biotechnol Biofuel 2011; 4:43.

530   doi:10.1186/1754-6834-4-43.

531   [16] Kim S, Gopalakrishnan K, Ceylan H. Moisture Susceptibility of Subgrade Soils Stabilized

532   by Lignin-Based Renewable Energy Co-product. J Transp Eng- ASCE 2012;138(11):1283-

533   1290. doi:10.1061/(ASCE)TE.1943-5436.0000097.

534   [17] Jahangiri M, Shahtaheri SJ, Adl J, Rashidi A, Kakooei H, Forushani AR, Nasiri G,

535   Ghorbanali A, Ganjali MR. Preparation of activated carbon from walnut shell and its

536   utilization for manufacturing organic-vapour respirator cartridge. Fresen Environ Bull

537   2012;21:1508-14.

538   [18] Alsultan A, Mijan A, Taufiq-Yap YH. Preparation of Activated Carbon from Walnut Shell

539   Doped La and Ca Catalyst for Biodiesel Production from Waste Cooking Oil. Mater Sci

540   Forum 2016;840:348-52. doi:10.4028/www.scientific.net/MSF.840.348.

541   [19] Rouquerol F, Rouquerol J, Sing K. Adsorption by powders and porous solids, principles,

542   methodology and applications. Academic Press. London: UK; 1999.

543   [20] Dubinin MM. Progress in surface and membrane science. Academic Press. New York:

544   USA; 1975.

545 [21] Barrett EP, Joyner LG, Halenda PP. The determination of pore volume and area

546   distributions in porous substances. I. Computations from nitrogen isotherms, J Am Chem

547   Soc 1951;73:373-80. doi: 10.1021/ja01145a126.

548 [22] Lecloux A, Pirard JP. The importance of standard isotherms in the analysis of adsorption

549   isotherms for determining the porous texture of solids. J Colloid Interf Sci 1979;70:265–81.

550   doi:10.1016/0021-9797(79)90031-6.

551 [23] Miladinović MR, Stamenković OS, Veljković VB, Skala UD. Continuous sunflower oil

552   methanolysis over quicklime in a packed-bed tubular reactor. Fuel 2015;154:301-7.

553   doi:10.1016/j.fuel.2015.03.057.

554 [24] Alba-Rubio AC, Alonso Castillo ML, Albuquerque MCG, Mariscal R, Cavalcante Jr CL,

555   López Granados M. A new and efficient procedure for removing calcium soaps in biodiesel

556   obtained using CaO as a heterogeneous catalyst. Fuel 2012;95:464–70.

557   doi:10.1016/j.fuel.2011.12.024.

558 [25] Hui Min P, Shahbaz K, Rashmi W, Mjalli F S, Hashim M A, Alnashef I M. Removal of

559   residual catalyst from palm oil-based biodiesel using new ionic liquids analogous. J Eng Sci

560   Technol 2015;4:35-49.

561 [26] Ceylan S, Topçu Y. Pyrolysis kinetics of hazelnut husk using thermogravimetric analysis

562   Bioresour Technol 2014;156:182–8. doi:10.1016/j.biortech.2014.01.040.

563 [27] Yang H, Yan R, Chen H, Lee DH, Zheng C. Characteristics of hemicellulose, cellulose and

564   lignin pyrolysis. Fuel 2007;86:1781–8. doi:10.1016/j.fuel.2006.12.013.

565   [28] Luque R, Pineda A, Colmenares JC, Campelo JM, Romero1 AA, Serrano-Ruiz JC, Cabeza

566   LF, Cot-Gores J. Carbonaceous residues from biomass gasification as catalysts for biodiesel

567   production. J Nat Gas Chem 2012;21:246–50. doi:10.1016/S1003-9953(11)60360-5.

568   [29] Osman AI, Ahmed AT, Johnston CR, Rooney D.W. Physicochemical characterization of

569   miscanthus and its application in heavy metals removal from wastewaters. Environ Prog

570   Sustainable Energy 2018;37(3):1058-67. doi: 10.1002/ep.12783.

571   [30] Vassilev SV, Vassileva CG, Song YC, Li WY, Feng J. Ash contents and ash-forming

572   elements of biomass and their significance for solid biofuel combustion. Fuel

573   2017;208:377–409. doi:10.1016/j.fuel.2017.07.036.

574   [31] Emeruwa E, Jarrige J, Mexmain J, Bernardin M. Application of mercury porosimetry to

575   powder (UO_2) analysis. J Nucl Mater 1991;184:53-8.

576   [32] Sharma M, Khan AA, Puri SK, Tuli D.K. Wood ash as a potential heterogeneous catalyst

577   for biodiesel synthesis. Biomass Bioenerg 2012;41:94-106.

578   doi:10.1016/j.biombioe.2012.02.017.

579   [33] Khelafi M, Kalloum S, Boulal A, Mansir N, Bakache Y, Taufiq-Yap YH.

580   Transesterification of Sunflower Oil Using Heterogeneous Catalyst Derived From Date

581   Seeds of South Algeria. Inter J ChemTech Res 2018;11:249-59.

582   [34] Dai YM, Chen KT, Wang PH, Chen CC. Solid-base catalysts for biodiesel production by

583   using silica in agricultural wastes and lithium carbonate. Adv Powder Technol

584   2016;27:2432–8. doi:10.1016/j.apt.2016.08.021.

585   [35] Ho WWS, Ng HK, Gan S, Tan SH. Valuation of palm oil mill fly ash supported calcium

586   oxide as a heterogeneous base catalyst in biodiesel synthesis from crude palm oil. Energy

587   Convers Manag 2014;88:1167–78. doi:10.1016/j.enconman.2014.03.061.

588   [36] Acchar W, Dultra EJV. Ceramic materials from coffee bagass ash waste, SpringerBriefs in

589   Applied Sciences and Technology, 2015.

590

FIGURE CAPTIONS

Fig. 1. TGA/DTA profile of walnut biochar.

Fig. 2. XRD patterns of (a) walnut shell biochar (b) walnut shell ash, (c) spent catalyst and (d) recalcined spent catalyst (800 ^{o}C for 2 h).

Fig. 3. Total intruded volume of Hg and pore size distribution of walnut shell ash for two consecutive runs.

Fig. 4. SEM images of (a,b) the fresh (walnut shell ash), (c,d) spent catalyst and (e,f) recalcined spent catalyst at magnification of 10,000 and 50,000.

Fig. 5. N_2 adsorption-desorption isotherm for walnut shell ash.

Fig. 6. The effect of (a) the catalyst loading (● - 0.5%, ▲ - 1%, ◆ - 2.5%, and ■ - 5%; initial methanol-to-oil molar ratio: 12:1) and (b) methanol-to-oil molar ratio (● - 6:1, ▲ - 12:1, and ■ - 18:1; catalyst loading: 1% of the oil weight) on FAME content (reaction temperature: 60 °C).

Fig. 7. The comparison of experimental (symbols) and predicted (dash line) TAG conversion degree (catalyst loading: ● - 0.5%, ▲ - 1%, ◆ - 2.5%, ■ - 5%; initial methanol-to-oil molar ratio: 12:1; reaction temperature: 60 °C).

Fig. 8. The comparison of the activities of walnut shell ash (catalyst loading: ▲ - 2.5% and ■ 5%) with NaOH (○) and KOH (△) (catalyst loading 1%) in the sunflower oil methanolysis at the initial methanol-to-oil molar ratio of 12:1 and the reaction temperature of 60 °C.

Fig. 9. Catalyst reuse at methanol-to-oil molar ratio12:1, catalyst load 5% and 60 °C (light grey – the FAME content within 10 min and dark grey – within 30 min of reaction): 1st reaction - with fresh catalyst, 2nd reaction - reuse of catalyst residue from 1st after reaction without reactivation, 3rd reaction - reuse of catalyst residue from 2nd reaction after recalcination at 800 °C for 2 h.

Fig. 10. Catalyst reuse after recalcination at 800 °C for 2h in each batch at methanol-to-oil molar ratio12:1, catalyst loading 5% and 60 °C (light grey – the FAME content within 10 min and dark grey – within 30 min).

Fig. 11. Elemental composition of walnut shell ash (black), spent catalyst (dark grey) and recalcined spent catalyst (light grey).

618 Table 1. Textural properties of walnut shell ash, the spent catalyst and the recalcined spent
619 catalyst.

Sample		Hg porosimetry					N$_2$ physisorption at 77 K		
		$V_{tot\text{-}Hg}$ [a] [mm^3/g]	ρ_{app} [g/cm^3]	ρ_{bulk} [b] [g/cm^3]	S_{Hg} [c] [m^2/g]	Porosity [%]	V_{mes} [mm^3/g]	V_{mic} [mm^3/g]	S_{BET} [m^2/g]
Walnut shell	Run 1	179	2.055	1.503	3.3	26.9	34	3	8.8
ash	Run 2	65	2.055	1.814	3.1	11.8			
Spent catalyst		-	-	-	-	-	14	1	3.1
Recalcined spent catalyst		-	-	-	-	-	3	<1	1.1

[a] Total intruded Hg volume obtained at the pressure of 200 MPa.

[b] Bulk density obtained at the atmospheric pressure.

[c] Specific surface area obtained for a cylindrical pore model.

620

621   Table 2 The apparent reaction rate constant of the sunflower oil methanolysis reaction over
622   walnut shell ash (reaction temperature: 60 °C).

Methanol-to-oil molar ratio	Catalyst loadings (%)	k_{app} (min^{-1})	R^2	MPRD[a] (%)
6:1	1	0.0968	0.971	2.57
	0.5	0.0309	0.983	9.60
12:1	1	0.0974	0.989	3.96
	2.5	0.1520	0.983	4.34
	5	0.2258	0.964	2.66
18:1	1	0.2232	0.979	2.58

623   [a] MRPD - Mean relative percent deviation

624

625 Table 3 The reusability of different ashes.

Catalyst	Catalyst preparation	The elements with high content present in the catalyst	Catalyst treatment prior reuse	Number of reuse cycle / status of catalytic activity	Leaching of catalytic active species	Reference
Boiler ash (empty fruit bunch ash)	Dried at 105 °C to constant weight	K, Si, Mg	Without treatment	2 / significant decrease of catalytic activity	Yes	[2]
	Calcined at 500, 700 and 900 °C			2 / significant decrease of catalytic activity		
Pine wood ash	Calcined at 800 °C for 4 h	Ca, O, K, Mg	Without treatment;	2 / significant decrease of catalytic activity	NR[a]	[18]
			Washed with acetone and ethanol and dried at 120 °C overnight prior to recalcination at 800 °C for 4 h	4 / partial recover of catalytic activity		
Lemna perpusilla Torrey ash	Calcined at 550 °C for 2 h	Si, K	Washed with petroleum ether and calcined at 550 °C for 1 h	3 / significant decrease of catalytic activity	Yes	[3]
Coconut husk ash	Calcined at 350 °C for 1 h	K, Ca, Si	Without treatment	1 / catalyst not active in repeated use	Yes	[1]
Tucumã peel ash	Calcined at 800 °C for 4 h	K, P, Ca, Mg	Washed with methanol	5 / gradual decrease of catalytic activity	No	[25]
Walnut shell ash	Traditional combustion to obtain char which further calcined at 800 °C to transform into the ash	Ca, K, Mg, Si	Without treatment	2 / significant decrease of catalytic activity in the repeated use	Yes	This work
			Recalcined at 800 °C for 2 h prior each cycle	4 /recover of catalytic activity		

626 [a]-Not reported

627

628   Table 4. Comparison of the used crude biodiesel purification methods.

Purification method	K+Na (ppm)	Ca+Mg (ppm)
Water washing	3.40	4.26
Alba Rubio et al.	1604	4.49
DES washing:		
Choline chloride:glycerol:ethylene glycol (1:2:1)	2704	6.47
Choline chloride:glycerol (1:2)	2838	7.58

629

630

631   Table 5. Characterization of FAMEs.

Properties	Water washed	EN 14214
Density (15 °C), kg/m^3	871	860-900
Acid value, mg KOH/g	0.51	0.50 max
Iodine value, g I$_2$/100 g	104	120 max
Water, mg/kg	484	500 max
Sodium/Potassium, ppm	3.40	5
Calcium/Magnesium, ppm	4.26	5
FAME, %	97.9	96.5 min

632

633
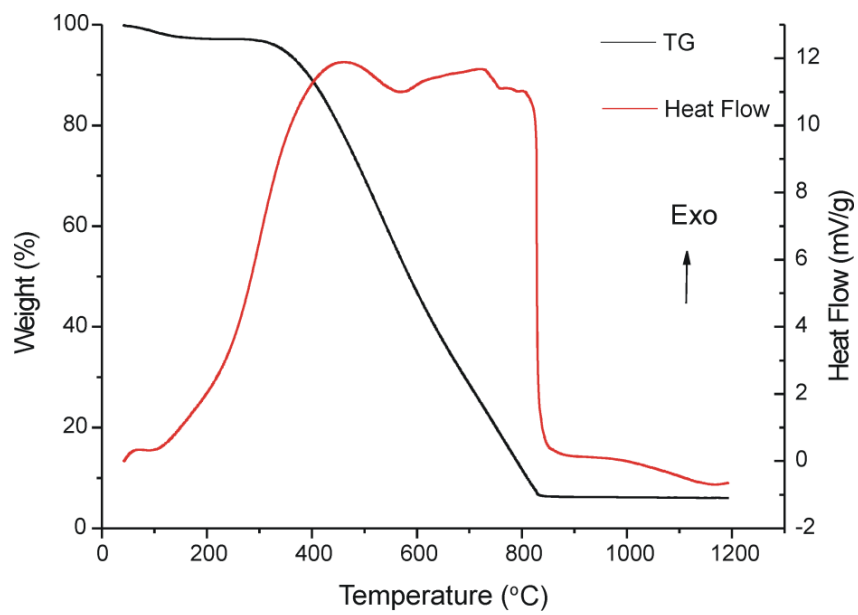
634

635   Fig. 1. TGA/DTA profile of walnut biochar.

636
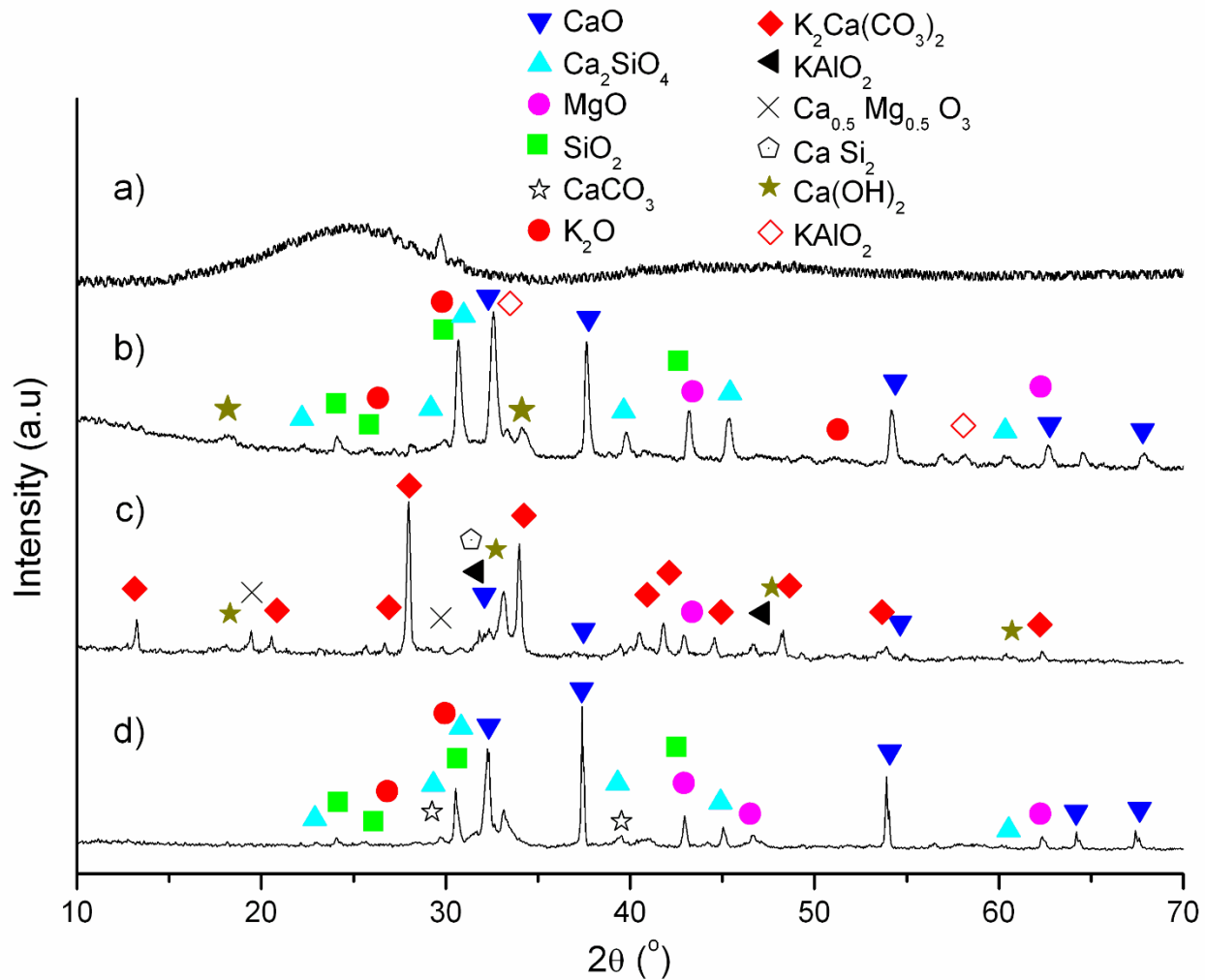
Fig. 2. XRD patterns of (a) walnut shell biochar (b) walnut shell ash, (c) spent catalyst and (d) recalcined spent catalyst (800 $^{\circ}$C for 2 h).
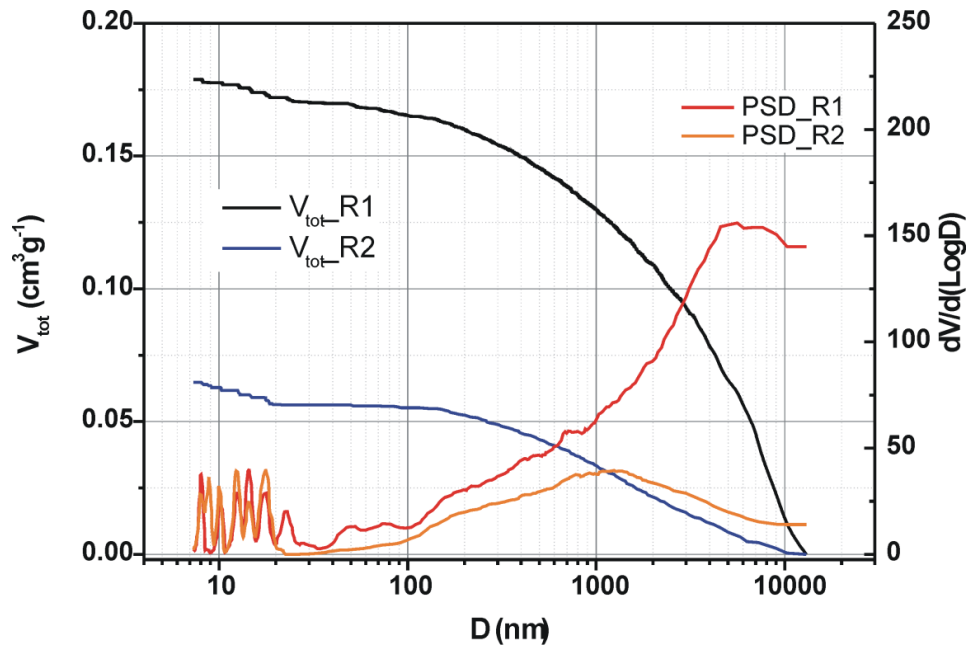
642

643   Fig. 3. Total intruded volume of Hg and pore size distribution of walnut shell ash for two
644   consecutive runs.

645

646
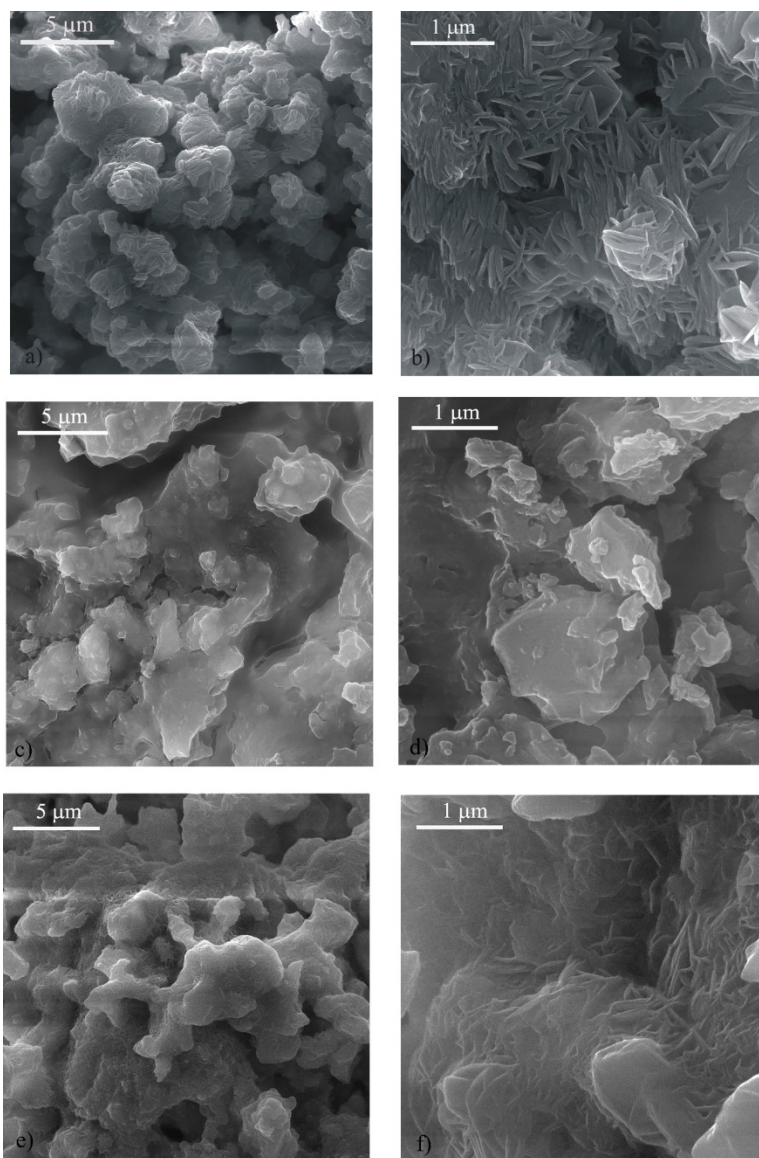
Fig. 4. SEM images of (a,b) the fresh (walnut shell ash), (c,d) spent catalyst and (e,f) recalcined

648 spent catalyst at magnification of 10,000 and 50,000.

649
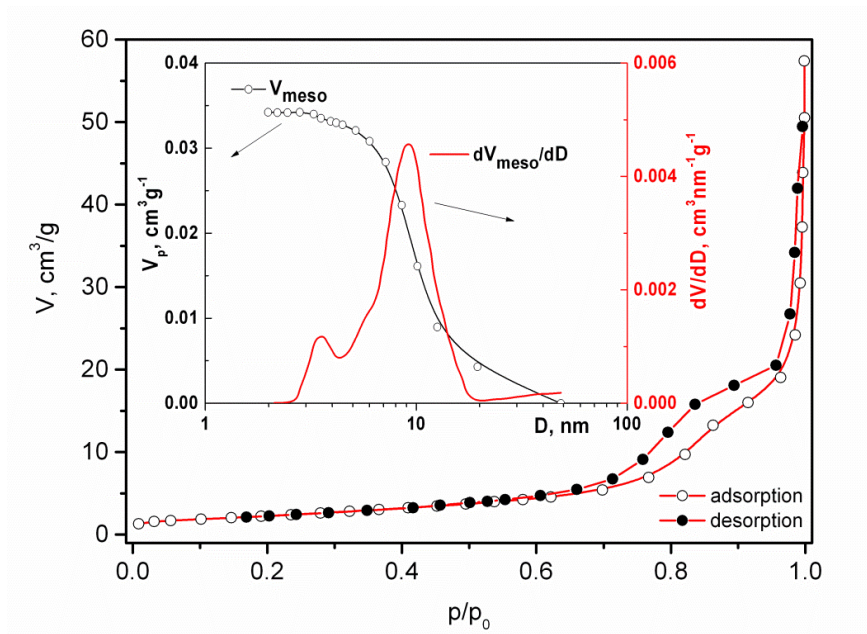
650

651   Fig. 5. N_2 adsorption-desorption isotherm for walnut shell ash.

652
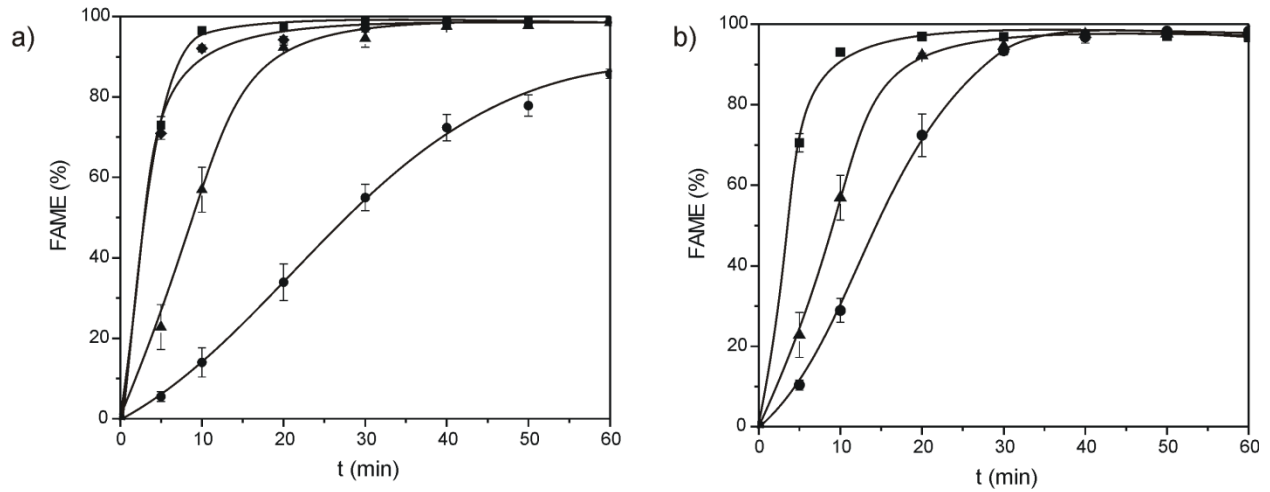
653

Fig. 6. The effect of (a) the catalyst loading (● - 0.5%, ▲ - 1%, ◆ - 2.5%, and ■ - 5%; initial methanol-to-oil molar ratio: 12:1) and (b) methanol-to-oil molar ratio (● - 6:1, ▲ - 12:1, and ■ - 18:1; catalyst loading: 1% of the oil weight) on FAME content (reaction temperature: 60 °C).

657
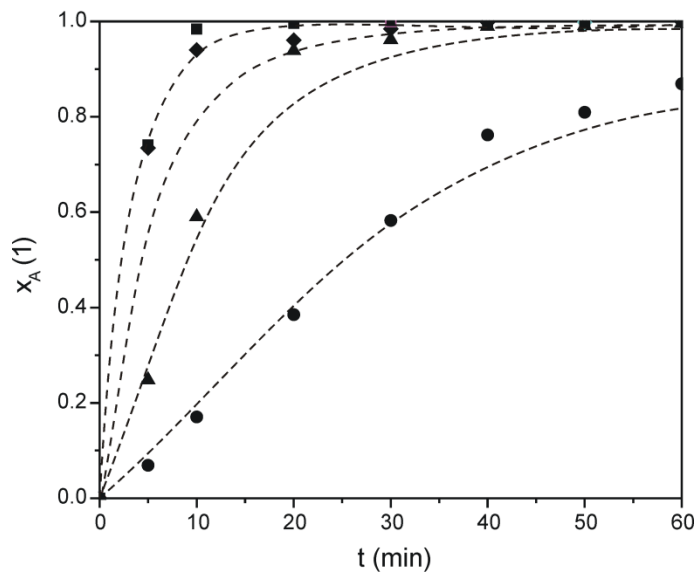
658

659

660   Fig. 7. The comparison of experimental (symbols) and predicted (dash line) TAG conversion
661   degree (catalyst loading: ● - 0.5%, ▲ - 1%, ◆ - 2.5%, ■ - 5%; initial methanol-to-oil molar
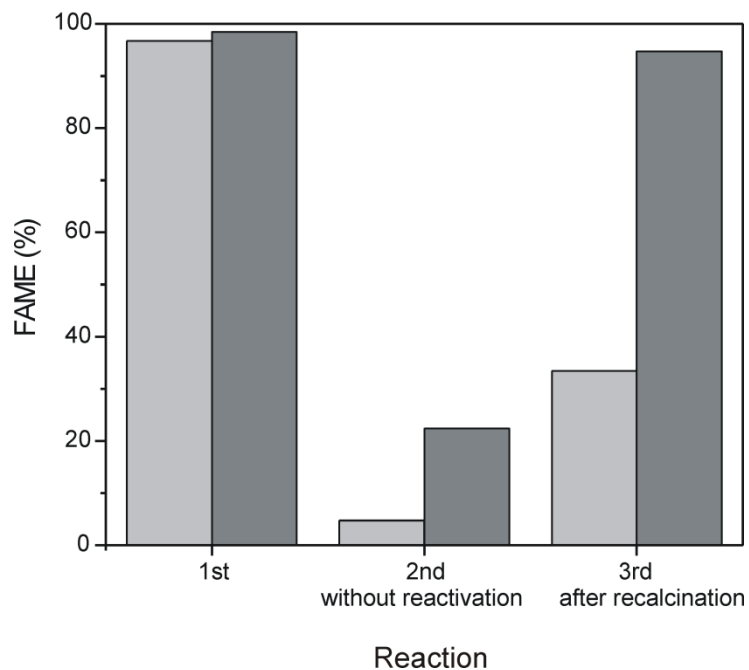662   ratio: 12:1; reaction temperature: 60 °C).

663
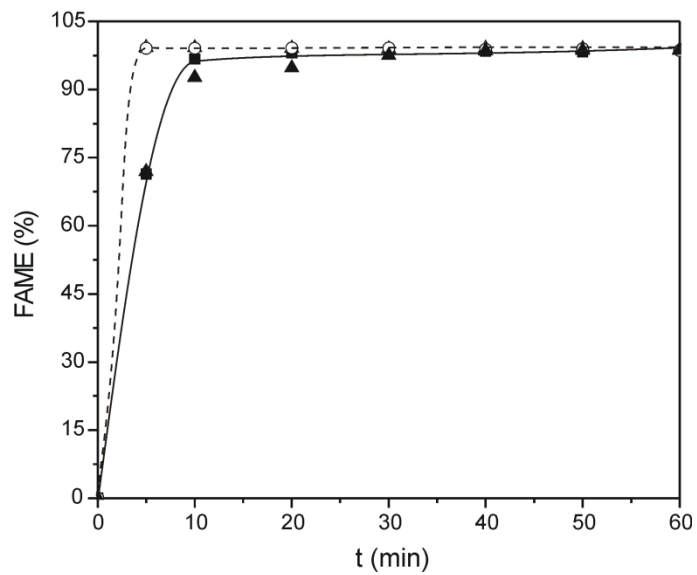
664

Fig. 8. The comparison of the activities of walnut shell ash (catalyst loading: ▲ - 2.5% and ■
5%) with NaOH (○) and KOH (△) (catalyst loading 1%) in the sunflower oil methanolysis at
the initial methanol-to-oil molar ratio of 12:1 and the reaction temperature of 60 °C.

668

669

Fig. 9. Catalyst reuse at methanol-to-oil molar ratio12:1, catalyst load 5% and 60 °C (light grey – the FAME content within 10 min and dark grey – within 30 min of reaction): 1st reaction - with fresh catalyst, 2nd reaction - reuse of catalyst residue from 1st after reaction without reactivation, 3rd reaction - reuse of catalyst residue from 2nd reaction after recalcination at 800 °C for 2 h.
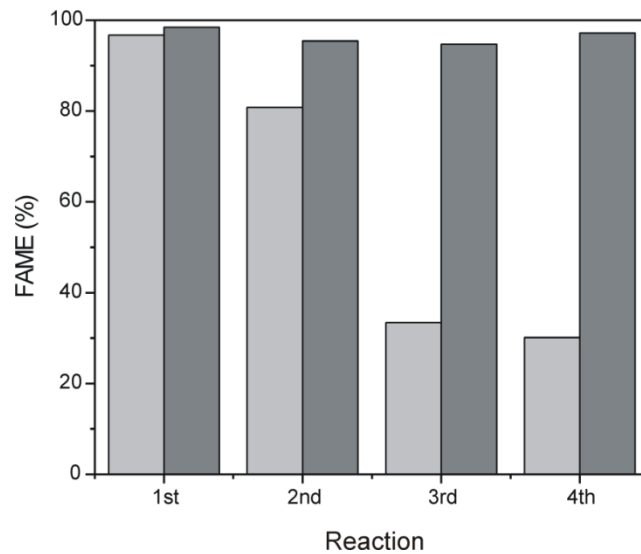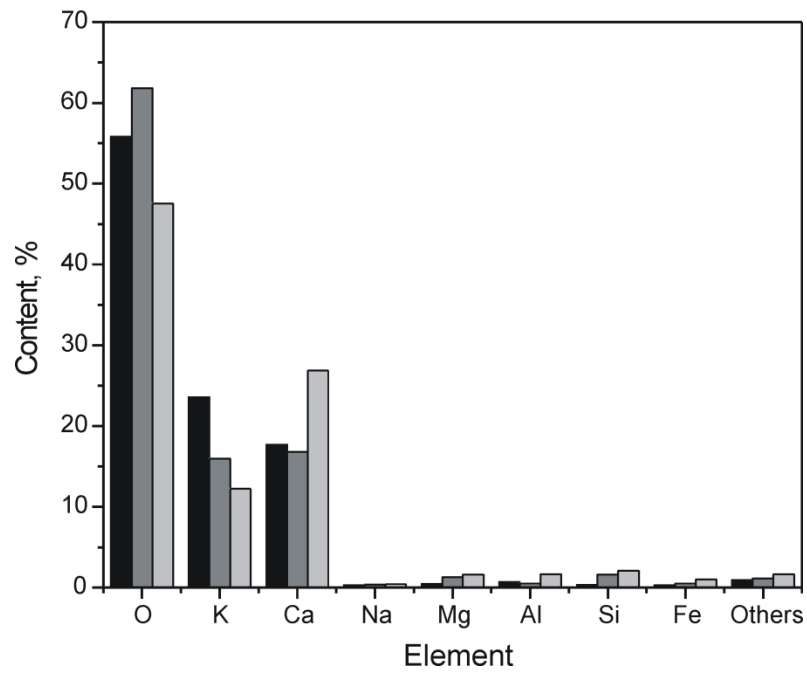
675

676 Fig. 10. Catalyst reuse after recalcination at 800 °C for 2h in each batch at methanol-to-oil molar
677 ratio12:1, catalyst loading 5% and 60 °C (light grey – the FAME content within 10 min and dark
678 grey – within 30 min).

679

680

681

682

683　Fig. 11. Elemental composition of walnut shell ash (black), spent catalyst (dark grey) and

684　recalcined spent catalyst (light grey)

685